Hybrid Resonant Half-Bridge DC/DC Converter With Wide Input Voltage Range

Bumyun Kim*, Sooa Kim*, Dong-Young Huh†, Jung-Hwan Choi†, and Minsung Kim*
*Pohang University of Science and Technology, Pohang, Gyeongbuk, South Korea
Email: minsung.kim@postech.ac.kr
†LG Innotek, Ansan, Gyeongki, South Korea

***Abstract*—Photovoltaic power conditioning systems (PCSs) requires a high-boost ratio over wide-input-range along with the isolation. This paper presents a hybrid resonant half-bridge dc/dc converter for photovoltaic power applications. This converter operates in a resonant half-bridge converter (RHBC) mode when the input voltage is higher than nominal input voltage. When the input voltage is lower than the nominal input voltage, the converter operates in a resonant boost (RB) mode in which the resonant half-bridge circuit on the secondary side boosts the secondary side resonant inductor current to achieve high boost-ratio. As a result, the proposed converter achieves high boost-ratio over wide-input-range with simple circuit structures. Detailed analysis of the converter operation is discussed along with the experiment using 600-W prototype to confirm the theoretical analysis and validity of the proposed converter.**

***Index Terms*—Photovoltaic, resonant half-bridge circuit, high step-up, wide input voltage range**

I. Introduction

Global interest toward renewable energy is steadily increasing. Among several renewable energy sources, photovoltaic (PV) source holds the biggest portion of the entire renewable energy due to its unlimited energy source, no polluting factors, and both high power density and efficiency [1–4]. In PV power systems, electrical energy generated from PV panel is modified and collected by PV modules. Grid-connected inverter then takes over the energy and delivers it to the utility grid. Nowadays, a module integrated converter (MIC) is setting the trend since it enables each PV module to only handle individual PV panel, which eventually weakens the mismatch problem caused by shadow effect [5–11].

Each PV module operates at both low and wide input voltage range. Thus, the MIC is required to not only have a high conversion ratio, but also have to handle the wide input voltage range to support effective maximum power point (MPP) tracking [12–14].

A resonant half-bridge converter (RHBC) [15–17] received considerable attention among the single-phase MIC topologies available for PV power systems due to its small number of components, and its potential for high efficiency. However, achieving high conversion ratio for RHBC is difficult because it basically operates as buck converter. Recently, a bridgeless structure based the hybrid resonant converter has been introduced [18, 19]. It achieves high conversion ratio by operating PWM resonant boost (RB) mode whenever the input voltage is lower than the nominal input. However, it requires four active power components on the secondary side.

In this paper, we propose a hybrid resonant half-bridge dc/dc converter. Proposed converter operates in RHBC mode when the input voltage is higher than the nominal input voltage. Soft switching technique is applied to the primary side switches to achieve high efficiency at this mode. Otherwise, it operates in RB mode which boosts the resonant inductor current by using the secondary side resonant half-bridge circuit. Thus, the proposed converter achieves the high boost ratio and high efficiency over a wide input voltage range. Experimental prototype was fabricated to validate the proposed converter.

The remainder of this study is organized as follows. The mode analysis of the proposed converter is described in Section II. Experimental results are presented in Section III, and the conclusions are drawn in Section IV.

II. Topology and System Description

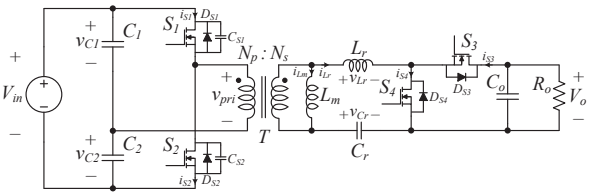

Fig. 1. Circuit diagram of the proposed converter.

The proposing converter of this paper is shown in Fig. 1. This converter consists of a primary side half-bridge circuit and a secondary side resonant half-bridge circuit, which operates in two classified modes: RHBC mode and RB mode.

Several assumptions are made to analyze the steady-state operation of the proposed converter:
1) the input capacitors C_1, C_2, and the output capacitor C_o are large enough, so the input/output voltages have no ripple voltage; $V_{C_1} = V_{C_2} = \frac{V_{in}}{2}$ because C_1 is set equal to C_2;
2) both primary and secondary switches S_1–S_4 are considered as ideal switches parallel with their body diodes and output capacitors;
3) the transformer T is an ideal transformer with primary winding turns N_p, secondary winding turns N_s, and magnetizing inductance L_m.

A. RHBC mode analysis

When the input voltage is higher than the nominal input voltage, the proposed converter operates in RHBC mode. Primary side switches operate in duty-control mode with constant phase of $\varphi = 180°$, including a short dead-time.

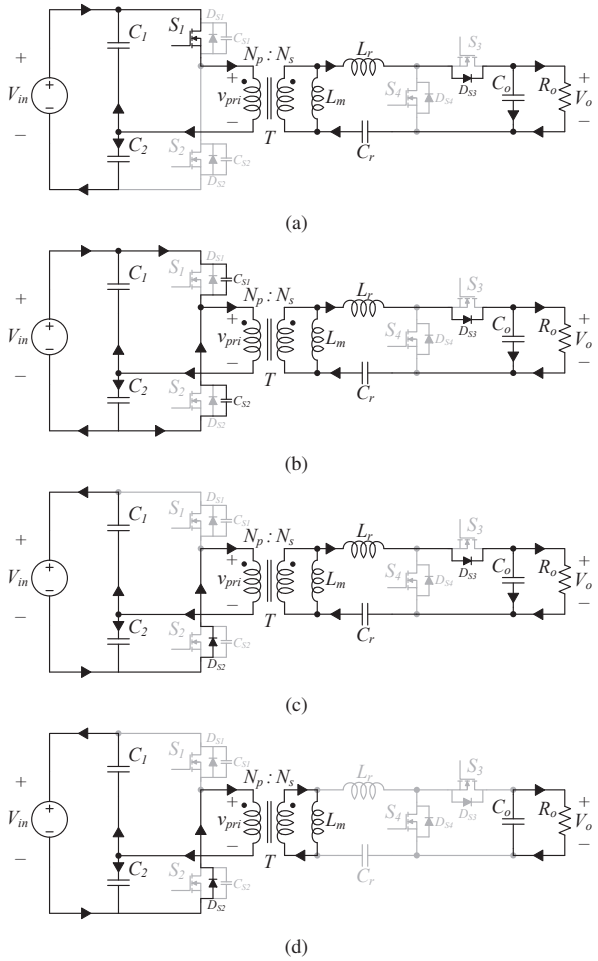

Fig. 2. Equivalent circuits during half switching period in RHBC mode. (a) Mode 1. (b) Mode 2. (c) Mode 3. (d) Mode 4.

Mode 1 [t_0, t_1]: At time t_0, the voltage across S_1 is zero and the primary side current i_{pri} flows through D_{S1}. S_1 is then turned on with zero-voltage-switching (ZVS). During this mode, the secondary side voltage is nV_{in} and i_{L_r} begins to flow through body diode D_{S3}. In this mode, the state equation of the circuit can be written as

$$L_r \frac{di_{L_r}(t)}{dt} = \frac{nV_{in}}{2} - V_0 + v_{C_r}(t), \tag{1}$$

$$i_{L_r}(t) = -C_r \frac{dv_{C_r}(t)}{dt}, \tag{2}$$

with $i_{L_r}(t_0) = 0$ and $v_{C_r}(t_0) = V_o/2 + \Delta V_{cr}$, where ΔV_{cr} is the voltage ripple of the resonant capacitor. Solving (1) and (2) then yields

$$i_{L_r}(t) = \frac{r_1}{Z_r} \sin\left[w_r(t - t_0)\right], \tag{3}$$

$$v_{C_r}(t) = V_0 - \frac{nV_{in}}{2} + r_1 \cos\left[w_r(t - t_0)\right], \tag{4}$$

where $r_1 = \frac{nV_{in} - V_0}{2} + \Delta V_{cr}$ is the radius of the circular path with the center at $(V_0 - \frac{nV_{in}}{2}, 0)$ as in Fig. 4. The operating point moves along the trajectory curve from A_1 to B_1 as shown in Fig. 4, and the resonant angular frequency w_r and the characteristic impedance Z_r are given by

$$w_r = \frac{1}{\sqrt{L_r C_r}}, \tag{5}$$

$$Z_r = \sqrt{\frac{L_r}{C_r}}. \tag{6}$$

Mode 2 [t_1, t_2]: At time t_1, S_1 is turned off and the current flows through both C_{S1} and C_{S2}, charging C_{S1} and discharging C_{S2}. After C_{S2} is fully discharged at time t_2, D_{S2} is conducted and the primary side current only flows throuhg D_{S2}. The primary side voltage v_{pri} drops from $\frac{V_{in}}{2}$ to $\frac{-V_{in}}{2}$ between t_1 and t_2. At this time, the trajectory path approximately stays at point B_1 as shown in Fig. 4.

Mode 3 [t_2, t_3]: From time t_2 to t_3, i_s, which flows through D_{S3}, continously drops to zero. When i_s reaches zero at time t_3, v_{pri} becomes zero and v_{C_r} reaches its minimum value. During this interval, the primary current only flows through D_{S2}, and the state equation of the circuit can be written as

$$L_r \frac{di_{L_r}(t)}{dt} = -\frac{nV_{in}}{2} - V_0 + v_{C_r}(t), \tag{7}$$

$$i_{L_r}(t) = -C_r \frac{dv_{C_r}(t)}{dt}, \tag{8}$$

with $i_{L_r}(t_1) \approx i_{L_r}(t_2) = \frac{r_2}{Z_r} \sin\alpha$ and $v_{C_r}(t_1) \approx v_{C_r}(t_2) = V_0 + \frac{nV_{in}}{2} - r_2 \cos\alpha$, where $\alpha = \sin^{-1}(\frac{r_1}{r_2} \sin(\pi - w_r(t_1 - t_0)))$. Solving (7) and (8) yields

$$i_{L_r}(t) = \frac{r_2}{Z_r} \sin\left[\alpha - w_r(t - t_2)\right], \tag{9}$$

$$v_{C_r}(t) = V_0 + \frac{nV_{in}}{2} - r_2 \cos\left[\alpha - w_r(t - t_2)\right], \tag{10}$$

where $r_2 = \frac{nV_{in} + V_0}{2} + \Delta V_{cr}$ is the radius of the circular path with center at $(V_0 + nV_{in}, 0)$ as in Fig. 4. The operating point moves along the trajectory curve from B_1 to A_2 as shown in Fig. 4.

Mode 4 [t_3, t_4]: During this mode, both primary side voltage and secondary side current are zero. The magnetizing current from L_m is reflected to the primary side, which holds the primary side current to have small non-zero value. This current flows through D_{S2}, therefore S_2 is turned on ZVS at time t_4. The trajectory path stays at point A_2 during this interval.

During the next half switching period, waveforms in the circuit are similar to Mode 1−4.

B. RB mode analysis

When the input voltage is lower than the nominal input voltage, the proposed converter operates in resonant boost mode. Primary side switches operate with constant phase of $\varphi = 180°$ with constant duty-ratio $D = 0.5$ including short dead-time.

Mode 1 [t_0, t_1]: At time t_0, the voltages across S_1

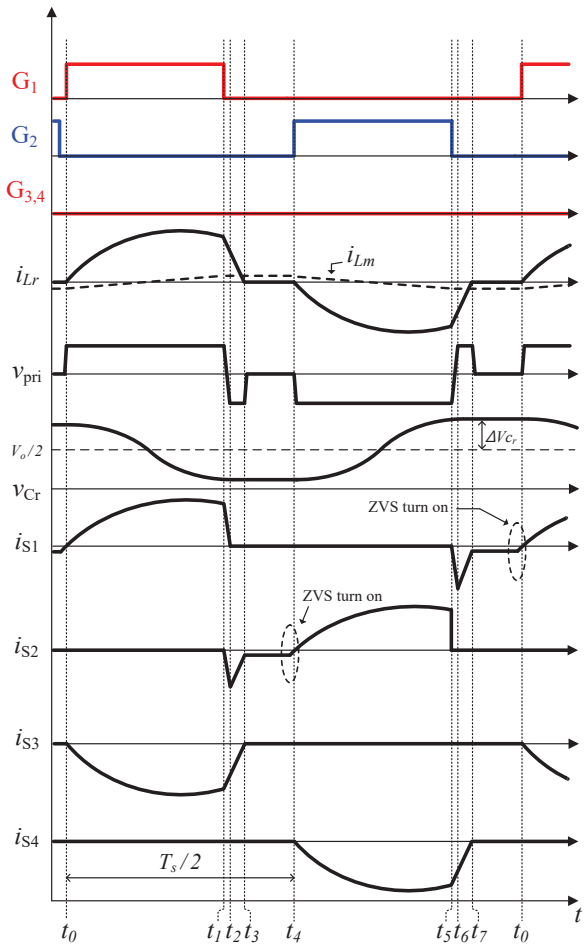

Fig. 3. Waveforms of the proposed converter in RHBC mode. G_1, G_2, G_3, and G_4 represents the gate signals of S_1, S_2, S_3, and S_4

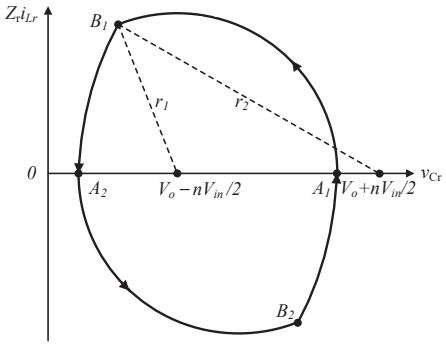

Fig. 4. State-plane trajectory in RHBC mode.

is zero, and the current begins to flow through D_{S1}. Thus, S_1 is turned on with ZVS. On the other hand, D_{S4} is conducted and S_4 is turned on with ZVS. Resonant inductor current i_{L_r} begins to flow from zero and v_{C_r} begins to decrease from its maximum value. During this interval, the input voltage source, the resonant inductor, and the resonant capacitor form an equivalent closed circuit which boosts the resonant inductor current following the sinusoidal waveform. The state equation

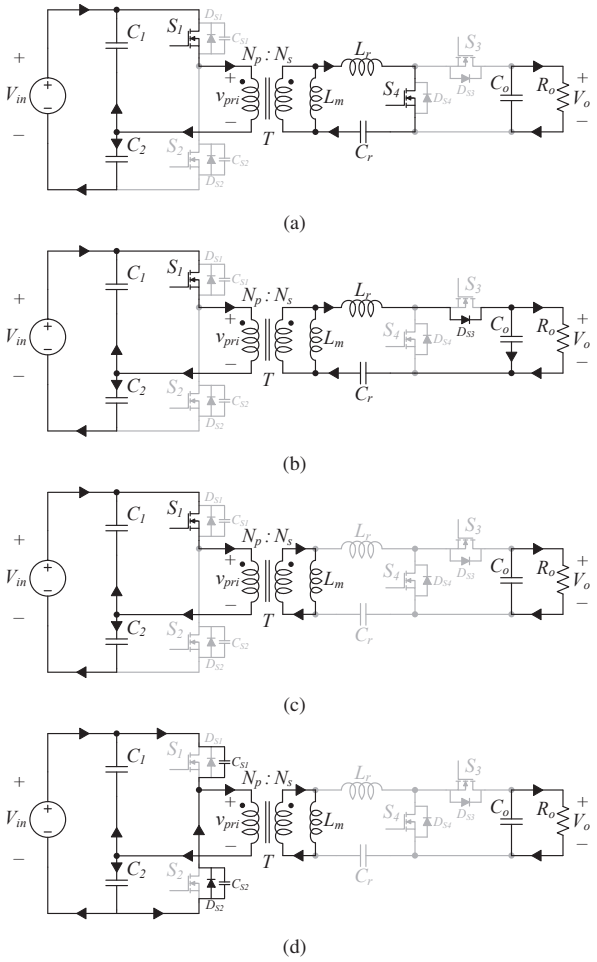

Fig. 5. Equivalent circuits during half switching period in RB mode. (a) Mode 1. (b) Mode 2. (c) Mode 3. (d) Mode 4.

corresponding to this equivalent circuit can be written as

$$L_r \frac{di_{L_r}(t)}{dt} = \frac{nV_{in}}{2} + v_{C_r}(t), \tag{11}$$

$$i_{L_r}(t) = -C_r \frac{dv_{C_r}(t)}{dt}, \tag{12}$$

with $i_{L_r}(t_0) = 0$ and $V_{C_r}(t_0) = V_o/2 + \Delta V_{cr}$. Solving (11) and (12) yields

$$i_{L_r}(t) = \frac{r_3}{Z_r} \sin\left[w_r(t - t_0)\right], \tag{13}$$

$$v_{C_{r1}}(t) = -\frac{nV_{in}}{2} + r_3 \cos\left[w_r(t - t_0)\right], \tag{14}$$

where $r_3 = \frac{nV_{in}+V_0}{2} + \Delta V_{cr}$ is the radius of the circular path with center at $(-\frac{nV_{in}}{2}, 0)$ as in Fig. 7. Here the operating point moves along the trajectory curve from A_1 to B_1 as in Fig. 7.

Mode 2 [t_1, t_2]: At time t_1, S_4 is turned off. The current on the secondary side then flows through D_{S3}. During this interval, the input voltage source, the resonant inductor, and the resonant capacitor form an equivalent closed circuit, and the resonant inductor current goes to zero following the sinusoidal waveform. The state

equation corresponding to this equivalent circuit can be written as

$$L_r \frac{di_{L_r}(t)}{dt} = nV_{in} - V_0 + v_{C_r}, \tag{15}$$

$$i_{L_r}(t) = -C_r \frac{dv_{C_r}(t)}{dt}, \tag{16}$$

with $i_{L_r}(t_1) = \frac{r_4}{Z_r}\sin\beta$ and $v_{C_r}(t_1) = V_0 - \frac{nV_{in}}{2} + r_4\cos\beta$, where $\beta = \sin^{-1}(\frac{r_3}{r_4}\sin[w_r(t_1 - t_0)])$. Solving (15) and (16) yields

$$i_{L_r}(t) = \frac{r_4}{Z_r}\sin\left[\beta + w_r(t - t_1)\right], \tag{17}$$

$$v_{C_{r1}}(t) = V_0 - \frac{nV_{in}}{2} + r_4\cos\left[\beta + w_r(t - t_1)\right], \tag{18}$$

where $r_4 = \frac{V_o - nV_{in}}{2} - \Delta V_{cr}$ is the radius of the circular path center at $(V_0 - \frac{nV_{in}}{2}, 0)$ as in Fig. 7. The operating point moves along the trajectory curve from B_1 to A_2 as shown in Fig. 7.

Mode 3 [t_2, t_3]: At time t_2, $i_{L_r} = 0$ and v_{C_r} is at its minimum. During this interval, the current that flows through S_1 is i_{Lm} reflected on the primary side, which is almost zero. Thus, at time t_3, switch S_1 gets turned off with nearly ZCS. Here, the trajectory path stays at point A_2 as shown in Fig. 7.

Mode 4 [t_3, t_4]: At time t_3, S_1 is turned off with almost ZCS and enters the dead-time zone. During this time, i_{Lm} appears as a current source to the primary side, which charges C_{S1} while discharging C_{S2}. After C_{S2} is fully discharged, D_{S2} is conducted, therefore, S_2 is turned on with ZVS at time t_4. The trajectory path still stays at point A_2 during this interval.

During the next half switching period, waveforms in the circuit are similar as with Mode 1−4.

III. Experimental Results

Experiment using a 600-W prototype has been conducted to evaluate the feasibility of the proposed converter. The prototype was designed to operate within input voltage range of $V_{in} = 45 - 75$ V, output voltage $V_o = 360$ V, and rated output power $P_o = 600$ W. At the nominal input voltage $V_{in,nom} = 60$ V, a full duty-ratio is utilized in RHBC mode to maximize the power conversion efficiency.

When $V_{in} = 75$ V, the converter operates in the RHBC mode (Fig. 8). As S_1 is turned on, i_{L_r} begins to increase. When S_1 is turned off and S_2 is turned on, i_{L_r} goes to 0 rapidly. When $V_{in} = 45$ V, the converter operates in the resonant boost mode (Fig. 9). While S_4 is turned on, the circuit boosts the resonant inductor current following the uphill part of the sinusoidal waveform. Then, the resonant inductor current decreases following the downhill part of the sinusoidal waveform.

The power conversion efficiency of the proposed converter was measured for a range of input/load conditions as shown in Fig. 10. The resonant boost mode efficiency is measured by Yokogawa WT330 digital power meter and the maximum value of the measured maximum efficiency is 95.5 % while the CEC weighted efficiency is 94.7 %.

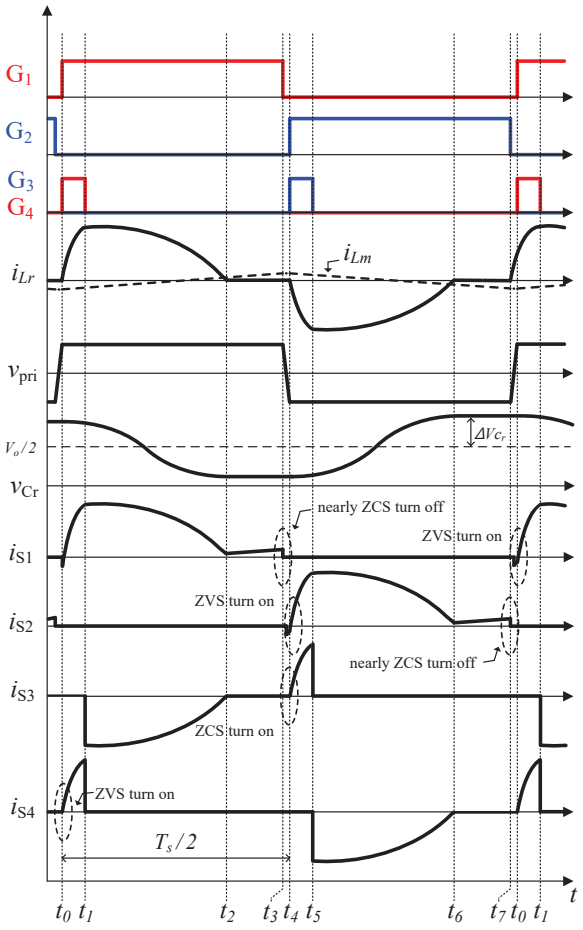

Fig. 6. Waveforms of the proposed converter in RB mode.

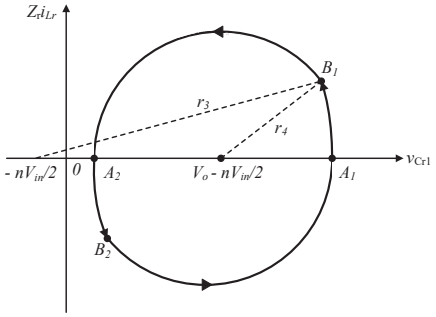

Fig. 7. State-plane trajectory in the resonant boost mode.

IV. Conclusion

In this paper, we propose a hybrid resonant half-bridge dc/dc converter for wide-input-range PV systems. When the input voltage is higher than the nominal input voltage, the proposed converter operates in RHBC mode which achieves a high efficiency by providing soft-switching technique to all the switches. Otherwise, it operates in RB mode that provides the step-up function by using a resonant half-bridge circuit at the secondary side. It can considerably extend the operating range of the converter as well as reduce the development cost and product size.

TABLE I
PARAMETERS AND COMPONENTS OF THE PROTOTYPE.

Parameters	Symbols	Value
Input voltage	V_{in}	45–75 V
Nominal voltage	V_{in_nom}	60 V
Output voltage	V_o	360 V
Output power	P_o	600 W
Switching frequency	f_s	100 kHz
Resonant frequency	f_r	88.6 kHz
Transformer turns ratio	N_p:N_s	11:69
Magnetizing inductance	L_m	2.33 mH
Resonant inductance	L_r	56.6 μH
Resonant capacitance	C_r	57 nF
Primary side capacitance	C_1, C_2	1000 μF
Filter inductance	L_f	200 μH
Filter capacitance	C_f	10 μH
Components	**Symbols**	**Part number**
Primary-side MOSFETs	$S_1 - S_2$	BSC026N
Secondary-side MOSFETs	S_3, S_4	UJC06505K
Transformer core	T	PQ3535

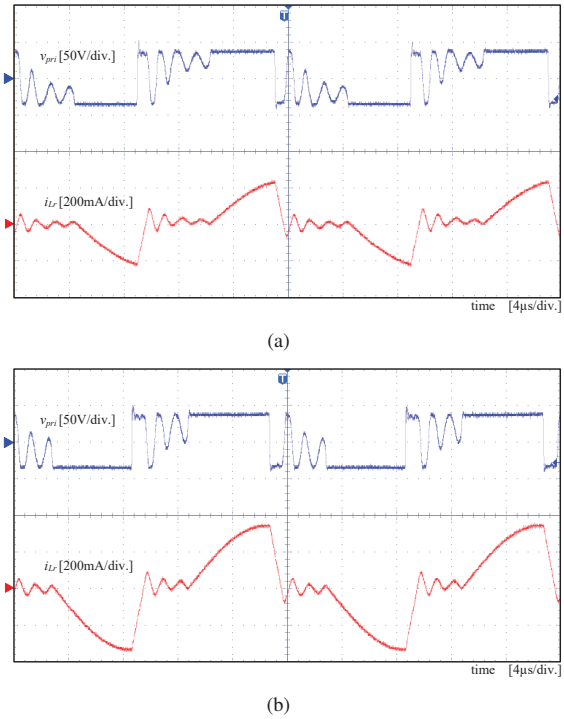

(a)

(b)

Fig. 8. Experimental waveforms of the RHBC mode when the input voltage is 75 V. (a) At half load. (b) At full load.

To confirm the validity of the proposed converter, 600-W prototype was built and tested.

ACKNOWLEDGMENT

This research was supported by the MSIP (Ministry of Science, ICT and Future Planning), Korea, under the "ICT Consilience Creative Program" (IITP-R0346-16-1007) supervised by the IITP (Institute for Information & communications Technology Promotion) and in part by the National Research Foundation of Korea (NRF) grant funded by MSIP (No. 2017R1C1B1003084).

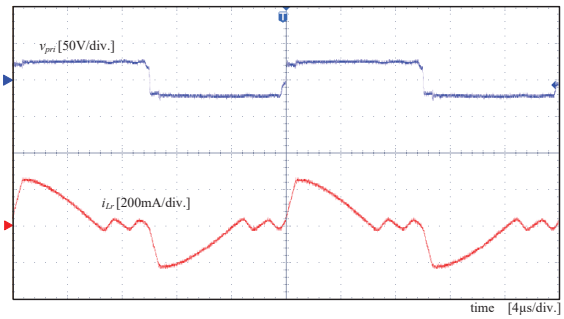

(a)

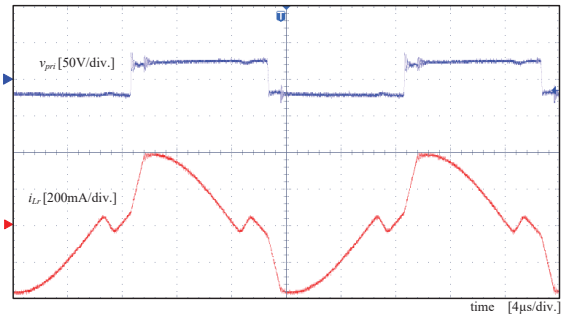

(b)

Fig. 9. Experimental waveforms of the resonant boost mode when the input voltage is 45 V. (a) At half load. (b) At full load.

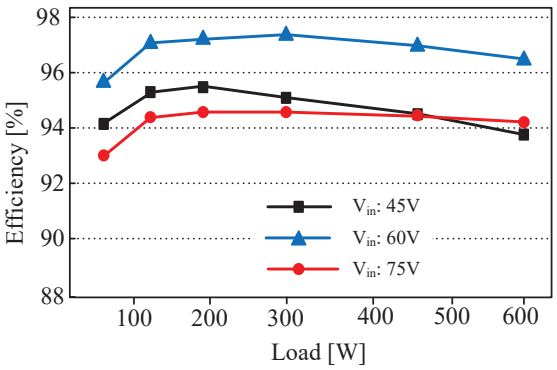

Fig. 10. Measured efficiency curves of the proposed converter for the various input range according to the output power.

REFERENCES

[1] M. N. Kabir, Y. Mishra, G. Ledwich, Z. Y. Dong, and K. P. Wong, "Coordinated control of grid-connected photovoltaic reactive power and battery energy storage systems to improve the voltage profile of a residential distribution feeder," *IEEE Trans. Ind. Informat.*, vol. 10, no. 2, pp. 967-977, 2014.

[2] Y. Yang, P. Enjeti, F. Blaabjerg, and H. Wang, "Wide-scale adoption of photovoltaic energy: Grid code modifications are explored in the distribution grid," *IEEE Ind. Appl. Mag.*, vol. 21, no. 5, pp. 21-31, 2015.

[3] S. Kouro, J. I. Leon, D. Vinnikov, and L. G. Franquelo, "Grid-connected photovoltaic systems: An overview of recent research and emerging PV con-

verter technology," *IEEE Ind. Electron. Mag.*, vol. 9, no. 1, pp. 47-61, 2015.

[4] D. Sun, B. Ge, W. Liang, H. Abu-Rub, and F. Z. Peng, "An energy stored quasi-Z-source cascade multilevel inverter-based photovoltaic power generation system," *IEEE Trans. Ind. Electron.*, vol. 62, no. 9, pp. 5458-5467, 2015.

[5] S. Harb, M. Mirjafari, and R. S. Balog, "Ripple-port module-integrated inverter for grid-connected PV applications," *IEEE Trans. Ind. Appl.*, vol. 49, no. 6, pp. 2692-2698, 2013.

[6] Y. Zhou, L. Liu, and H. Li, "A high-performance photovoltaic module-integrated converter (MIC) based on cascaded quasi-Z-source inverters (qZSI) using eGaN FETs," *IEEE Trans. Power Electron.*, vol. 28, no. 6, pp. 2727-2738, 2013.

[7] S. H. Lee, W. J. Cha, B. H. Kwon, and M. Kim, "Discrete-time repetitive control of flyback CCM inverter for PV power applications," *IEEE Trans. Ind. Electron.*, vol. 63, no. 2, pp. 976-984, 2016.

[8] S. Kim, S. H. Lee, J. S. Lee, and M. Kim, "Dual-mode flyback inverters in grid-connected photovoltaic systems," *IET Renew Power Gen*, vol. 10, no. 9, pp. 1402-1412, 2016.

[9] H. Kim, J. S. Lee, J. S. Lai, and M. Kim, "Iterative learning controller with multiple phase-lead compensation for dual-mode flyback inverter," *IEEE Trans. Power Electron.*, vol. 32, no. 8, pp. 6468-6480, 2017.

[10] A. Chub, D. Vinnikov, R. Kosenko, and E. Liivik, "Wide input voltage range photovoltaic micro-converter with reconfigurable buck–boost switching stage," *IEEE Trans. Ind. Electron.*, vol. 64, no. 7, pp. 5974-5983, 2017.

[11] B. Han, J. S. Lee, and M. Kim, "Repetitive controller with phase-lead compensation for Cuk CCM inverter," *IEEE Trans. on Ind. Electron.* (Accepted for publication, DOI: 10.1109/TIE.2017.2739678)

[12] H. Hu, X. Fang, F. Chen, Z. J. Shen, and I. Batarseh, "A modified high-efficiency LLC converter with two transformers for wide input-voltage range applications," *IEEE Trans. Power Electron.*, vol. 28, no. 4, pp. 1946-1960, 2013.

[13] T. LaBella, W. Yu, J. S. Lai, M. Senesky, and D. Anderson, "A bidirectional-switch-based wide-input range high-efficiency isolated resonant converter for photovoltaic applications," *IEEE Trans. Power Electron.*, vol. 29, no. 7, pp. 3473-3484, 2014.

[14] S. Lim, J. Ranson, D. M. Otten, and D. J. Perreault, "Two-stage power conversion architecture suitable for wide range input voltage," *IEEE Trans. Power Electron.*, vol. 30, no. 2, pp. 805-816, 2015.

[15] H. Sarnago, O. Lucia, A. Mediano, and J. M. Burdio, "Analytical model of the half-bridge series resonant inverter for improved power conversion efficiency and performance," *IEEE Trans. Power Electron.*, vol. 30, no. 8, pp. 4128-4143, 2015.

[16] S. H. Ryu, D. G. Woo, M. K. Kim, and B. K. Lee, "Analysis and design of modified half-bridge series-resonant inverter with dc-link neutral-point-clamped cell," *IEEE Trans. Power Electron.*, vol. 31, no. 3, pp. 2282-2295, 2016.

[17] Y. Jeong, J. K. Kim, J. B. Lee, and G. W. Moon, "An asymmetric half-bridge resonant converter having a reduced conduction loss for DC/DC power applications with a wide range of low input voltage," *IEEE Trans. Power Electron.*, vol. 32, no. 10, pp. 7795-7804, 2017.

[18] X. Zhao, L. Zhang, R. Born, and J. S. Lai, "A high-efficiency hybrid resonant converter with wide-input regulation for photovoltaic applications," *IEEE Trans. Ind. Electron.*, vol. 64, no. 5, pp. 3684-3695, 2017.

[19] J. Liu, K. W. Chan, C. Y. Chung, N. H. Chan, M. Liu, and W. Xu, "Single-stage wireless-power-transfer resonant converter with boost bridgeless power-factor-correction rectifier," *IEEE Trans. Ind. Electron.*, (Accepted for publication, DOI: 10.1109/TIE.2017.2745471)